Progress In Electromagnetics Research C, Vol. 128, 231–246, 2023

Design and Development of Sextuple Band Reject UWB-MIMO Antenna for Wireless Applications

Sadineni R. Babu[1, *] and Puttaraje G. Dinesha[2]

Abstract—In this manuscript, quad port highly isolated sextuple-band notched ultra-wideband (UWB) multiple input multiple output (MIMO) antenna is designed and experimentally investigated. The suggested design employs four antenna elements fabricated over a Rogers RT Duroid 5880 substrate and placed orthogonal to each other by deploying polarization diversity technique for good isolation. By combining polarization diversity technique with a fan-shaped de-coupler isolation could be improved even more. meliorated frequency selectivity of notch bands can be accomplished by loading each antenna element with four U-shaped slots and C-shaped stubs adjacent to the feed line to exhibit band rejection of 3.18–3.51 GHz (9.86%), 3.71–3.99 GHz (7.27%), 4.59–4.76 GHz (3.63%), 5.18–5.34 GHz (3.04%), 7.47–7.74 GHz (3.55%), and 9.29–9.55 GHz (2.76%) to surmount the possible intrusion from WiMAX, C-band, INSAT, WLAN, X-band, and radio navigation (RN) band. Besides, an RLC equivalent circuit has been examined by correlating with the outcome of the reported notch band UWB-MIMO antenna that evinces highly selective notch bands. The suggested antenna works in the frequency range of 2.1–11.2 GHz which is suitable for UWB applications. Simulation and experimental validation is done to analyze the response of the suggested antenna with respect to notch frequencies, current distributions, peak gain, radiation patterns, envelope correlation coefficient, diversity gain, mean effective gain, total active reflection coefficient, channel capacity loss, and multiplexing efficiency.

1. INTRODUCTION

In the year 2002, Federal Communications Commission (FCC) granted permission for unlicensed usage of ultra-wideband (UWB) frequency that extends from 3.1 to 10.6 GHz. It was meant for radar applications, but gradually it is getting utilized for high-speed data transmissions [1]. UWB antennas became popular for its benefits such as high data rate and channel capacity. However, UWB antennas suffer from multipath fading [2]. Combining UWB with multiple input multiple output (MIMO) antenna technology can overcome multipath fading apart from increasing transmission capability and reliability [3]. In MIMO, numerous antennas are used at transmission side and receiving side which escalates reliability. Because several antennas are present, mutual coupling is predominant. In order to mitigate mutual coupling researchers have proposed various techniques like neutralization lines [4-7], parasitic structures [8–10], defected ground structure (DGS) [11], de-couplers [12–15], and stubs [16]. The most important concern in UWB antennas is the interference caused by various narrow band systems. Sharing frequency bands is the prime reason for this interference. Some of the narrow bandwidth systems already existing in the UWB frequency bands are WiMAX (3.3–3.8 GHz), C-band (3.7–4.2/5.925–6.425 GHz), INSAT (4.5–4.8 GHz), WLAN (5.15–5.85 GHz), and X-band (7.7–8.4 GHz). One potential solution for rejecting these frequencies is to use band stop filters at the end of the antenna system. But this will enhance the complexity of the antenna system. Hence, achieving notch

Received 22 November 2022, Accepted 28 December 2022, Scheduled 16 January 2023
* Corresponding author: Sadineni Ramesh Babu (srameshbabu2022@gmail.com).
[1] Department of ECE, R.V.R & J.C College of Engineering, Guntur 522019, India. [2] Department of ECE, Dayananda Sagar College of Engineering, Bengaluru-560078, India.

characteristics and maintaining less complexity in implementation is a challenging task. Consequently, a multi-band rejection antenna is necessary for the elimination of disruptive frequencies. Many authors have proposed various techniques for the generation of single, dual, triple, quadruple, and penta-band notch characteristics. In this article, by loading slots on the patch and using stubs beside feed line notch frequencies are generated which essentially removes interference from narrow band systems. A MIMO antenna array that employs two quasi-self-complementary (QSC) antenna elements with rejection band at WLAN system is implemented with the aid of bent slits on each radiator [17]. In [18], the authors present a miniaturized octagon-shaped UWB-MIMO antenna with the mitigation of WLAN frequency by using a C-shape slot over the patch along with high isolation. A miniature and high performance UWB-MIMO antenna with a band filter design over the ground plane in order to alleviate mutual coupling is presented in [19]. A highly isolated MIMO diversity antenna with the help of a stepped stub as decoupling element and band rejection capability is introduced in [20]. In [21], a compact UWB-MIMO antenna with enhanced separation by utilizing neutralization line and dual notch behavior is accomplished. A two-port compact UWB-MIMO antenna array is investigated in [22], where dual band notches are attained with the aid of slots and a T-shaped stub. In [23], a UWB antenna integrated with slots along with an electromagnetic band-gap structure (EBG) structure is investigated. In [24–28], numerous miniature UWB-MIMO antennas with enhanced separation and tri-band suppression features are implemented. In [29], a quad notch band two-port UWB-MIMO antenna is introduced with two inverted L-shaped slots along with an EBG pair in order to achieve four notches. In [30], a miniature four port MIMO antenna with on demand WLAN rejection is explored.

Gaps Identified from the Related Works:

1. Most of the designs reported in existing literature are limited to the rejection of single, dual, triple, and quad band notches only.
2. Most MIMO antennas use DGS to enhance isolation. Yet isolation is not less than −20 dB for the whole operating bandwidth, and interelement separation is also more.
3. Most MIMO antennas existing in the literature have only two ports.
4. Most of the MIMO antennas were not investigated with equivalent circuit analysis and all the diversity performance metrics.

It is indispensable to eliminate critical interfering bands within UWB frequency range for the mitigation of interference to insignificant level. For better reliability, four port UWB-MIMO antennas with enhanced isolation are necessary. Hence, in this article, a four port and highly isolated hexa-band suppressed MIMO antenna for UWB applications is proposed. Novelty of the proposed design is achieving higher number of notches within UWB frequency range with rejection sharpness control in addition to high port to port isolation less than −20 dB throughout the operating bandwidth required for MIMO systems.

Contributions of the Proposed Work:

Listed below are the key features of the reported work to overcome the research gaps:

1. The effectual and straightforward UWB design with partial ground attains a reflection coefficient curve less than −18 dB for the entire operating bandwidth.
2. The controllable hexa-band rejection characteristics are attained with the help of four U-shaped slots on the patch and a C-shaped stubs adjacent to feed line.
3. The proposed UWB-MIMO antenna is experimentally evaluated with respect to peak gain, radiation patterns, and radiation efficiency.
4. The proposed UWB-MIMO antenna is evaluated with respect to diversity characteristics such as envelope correlation coefficient (ECC), diversity gain (DG), mean effective gain (MEG), total active reflection coefficient (TARC), channel capacity loss (CCL) and multiplexing efficiency (ME).

2. ANTENNA DESIGN AND ANALYSIS

2.1. Design Approach for Achieving UWB Characteristics

The steps followed in the design sequence of the UWB antenna and its return loss curves (carried out by CST MW Studio 2018) are depicted in Fig. 1. The suggested UWB antenna is made of copper material and printed on a Rogers RT Duroid 5880 substrate with permittivity 2.2, thickness 1.6 mm, and loss tangent of 0.0009. The copper foil has a conductivity of $5.8e^{+007}$ S/m and thickness 0.035 mm. A rectangular radiator has been implanted initially over the substrate along with the whole ground plane as depicted in antenna#1. As can be seen from Fig. 1, it is observed that the operating bandwidth is narrower at high frequency only. In order to escalate the impedance bandwidth, length of the ground is reduced to ($Lg = 10.5$ mm) as shown in Antenna#2. This impact improves the lower frequency band, boosting the upper. Antenna#2 with partial ground plane performs dual band operation from 2.56–5.52 GHz and 6.46–9.43 GHz. To enhance impedance bandwidth even more, symmetrical square slots have been etched on the rear side of the patch along with a groove on a partial ground plane. In comparison with antenna#2, the electrical length of the antenna is increased by introducing square incisions at the bottom corners of the radiator (Antenna#3), resulting in a wider bandwidth and better impedance matching.

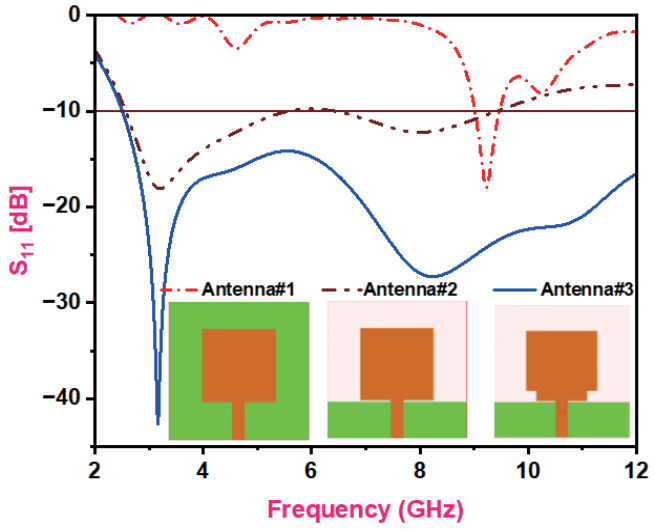

Figure 1. Simulated return loss characteristics of various patch antennas.

As is evident, from Fig. 1. Antenna#3 has a frequency range of operation that is well suited to the needs of a UWB system, spanning from 2.1 to 11.2 GHz. The optimized dimensional parameters of the suggested band suppressed UWB-MIMO antenna are mentioned in Table 1.

2.2. Methodology for Obtaining Notch Band Characteristics

Within UWB frequency range, various narrow bands also exist like WiMAX, C-band, INSAT, WLAN, X-band, and Radio navigation band. Due to spectrum sharing narrow band system always causes interference to UWB systems. In order to mitigate this interference, various notch techniques, such as creating slots and stubs, must be incorporated after the realization of UWB characteristics from the reported antenna system.

Figure 2(a) highlights the reported hexa-band suppressed UWB antenna loaded with four U-shaped slots and two C-shaped stubs beside feed-line. Here four U-shape slots are loaded on the patch to counter WiMAX band at 3.41 GHz, downlink C-band at 3.84 GHz, INSAT at 4.67 GHz, and WLAN at 5.26 GHz. Finally, a pair of C-shaped stubs beside feed line will provide notch frequencies at 7.61 GHz and 9.44 GHz to suppress the interference from X-band downlink and radio navigation bands, respectively. Fig. 2(b)

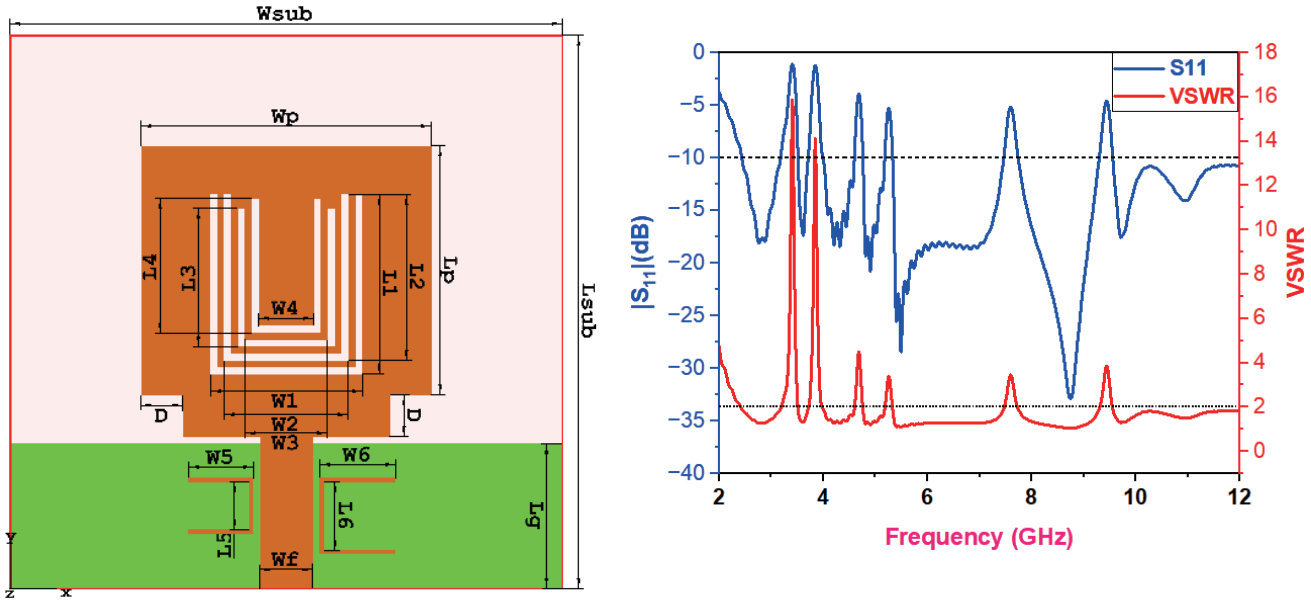

Figure 2. (a) Geometry of the suggested hexa-notch band UWB antenna. (b) Simulated S_{11} and VSWR characteristics.

illustrates the variation of return loss and VSWR against frequency for the proposed UWB notch band antenna. The return loss characteristics demonstrate that the proposed UWB antenna exhibits six notch frequencies within UWB frequency range along with an operating bandwidth extending from 2.1 to 11.2 GHz. The total length of each slot is determined by the formulae below.

$$f_n^i = \frac{co}{2L_{slot}^i\sqrt{\varepsilon_{eff}}} \tag{1}$$

$$L_{slot}^i = 2L_i + W_i \tag{2}$$

$$\varepsilon_{eff} = \frac{\varepsilon_r + 1}{2} \tag{3}$$

Here, C_0 is the free space light velocity, ε_{eff} the effective dielectric constant, ε_r the relative permittivity, and f_n^i the central notch frequency of the corresponding band.

2.3. Parametric Study

Depiction and description of comparative return loss characteristics helps understand rejection process sharpness control. Return Loss characteristics for each rejection band created by varying respective band notch element dimensions are illustrated in Fig. 3. For U-shaped slots L_1, L_2, L_3, L_4, W_1, W_2, W_3, and W_4 are the crucial parameters. At certain frequencies, the currents flowing through opposite sides of U-shaped slots are going in opposite directions, resulting in notch band characteristics. Parametric optimization is performed individually for each notch element by varying only one parameter while other design factors remain constant. Figs. 3(a)–(f) show S_{11}/S_{22} (dB) plots for the reported hexa-notch band UWB antenna. From Figs. 3(a)–(f), it can be inferred that when each notching structure's overall length increases, the intended stopband is relocated towards the lower frequency band. Similar to this, a shorter-length notching structure moves the intended stopband toward the higher frequency end. This is supported by Equations (1)–(3), where the relationship between the total length and desired notch frequency is inverse. Additionally, it has been shown that all notch frequencies are essentially independent of one another. Therefore, by adjusting the sizes and locations of the relevant band-notch components, the required notch frequency and bandwidth may be achieved.

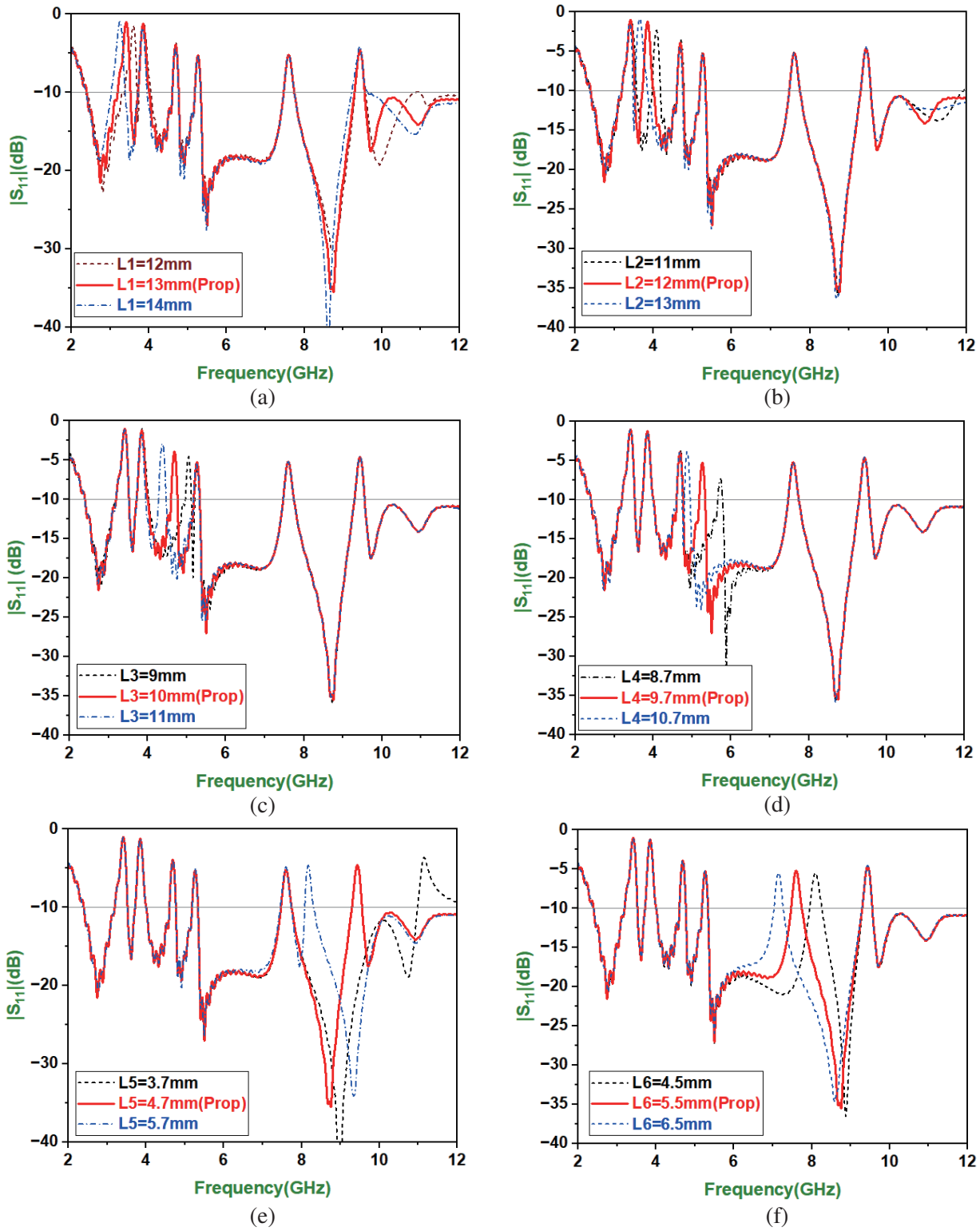

Figure 3. Simulated S_{11} plot for variation in (a) length of outer slot (slot-1) (b) length of slot-2 (c) length of slot-3 (d) length of innermost slot (e) length of left C-shaped stub (f) length of right C-shaped stub.

2.4. Design of Quad-Port UWB MIMO Antenna

The notch band UWB antenna presented in Fig. 2(a) has been chosen to model a 4×4 MIMO antenna system, as depicted in Fig. 4. The total footprint of the reported quad-port UWB MIMO antenna is $78 \times 78 \times 1.6\,\text{mm}^3$ or $0.55\lambda \times 0.55\lambda_0 \times 0.011\lambda_0$ and is integrated with four monopole antenna elements arranged orthogonal to each other by exploiting polarization diversity phenomenon. An in-depth investigation reveals an adequate diversity performance at isolation augmentation level, which elucidates the primary rationale behind orthogonal selection of (Ant1–Ant2), (Ant3–Ant4), (Ant1–Ant3), (Ant2–Ant4), (Ant2–Ant3), and (Ant1–Ant4) pairs to maintain good isolation among antenna elements. To accomplish isolation even more among antenna elements, a fan-shaped decoupling element is integrated at the rear side of the substrate as depicted in Fig. 4(b). The optimized dimensional parametric values of the suggested UWB-MIMO antenna are illustrated in Table 1.

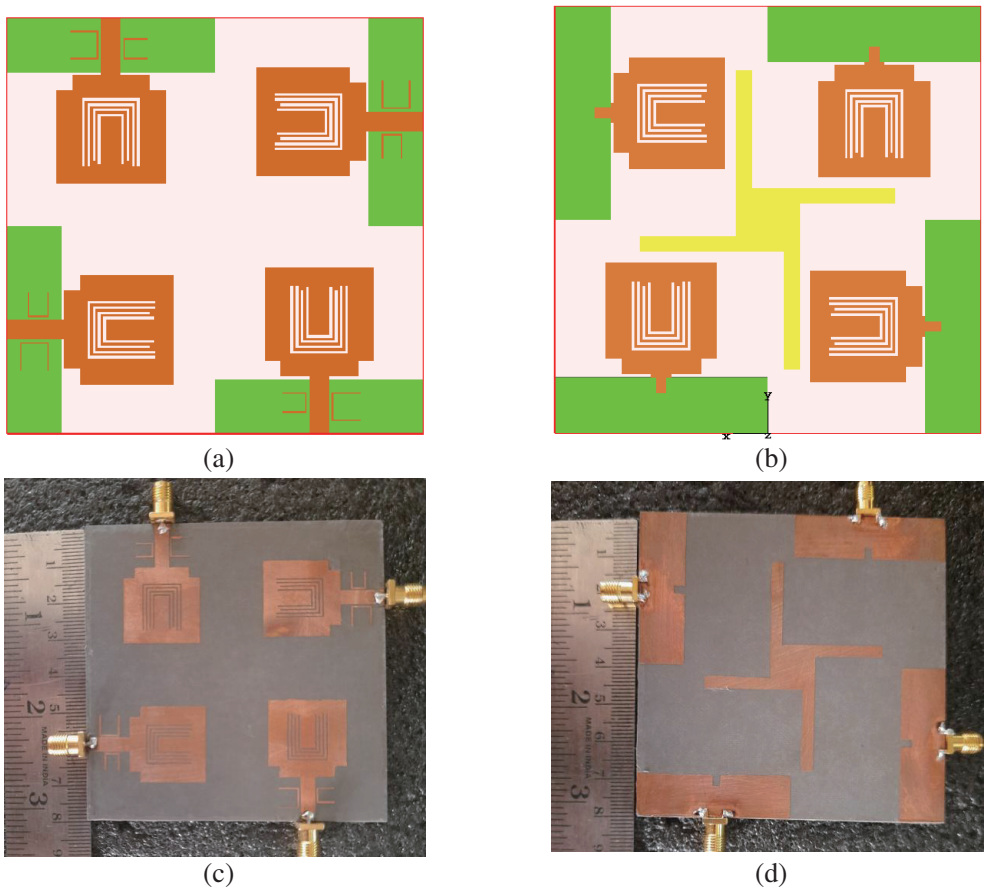

Figure 4. Reported quad port UWB-MIMO antenna (a) top layer (b) bottom layer (c) Fabricated model top side (d) Fabricated model bottom side.

Table 1. Optimized dimensional parameters of the proposed MIMO antenna.

W_{sub}	L_{sub}	W_p	L_p	W_f	L_f	D	W_1	W_2	W_3	W_4
39	39	21	18	3.8	11	3	11	9	7	5
W_5	W_6	L_1	L_2	L_3	L_4	W_g	L_g	L_5	L_6	-
4.7	6	13	12	10	9.7	39	10.5	4.7	5.5	-

2.4.1. Equivalent Circuit Analysis

In this section, band-rejection characteristics will be further examined by demonstrating an RLC equivalent circuit for the suggested UWB-MIMO antenna. Initial conceptualization of the principle of an equivalent RLC circuit model relies on the impedance characteristics of the designed UWB notch band antenna when port1 is stimulated, and remaining ports are terminated with 50 Ω loading as shown in Fig. 5. At the central notch frequencies of 3.41, 3.84, 4.67, 7.61, and 9.44 GHz, the real part component is close to 50 Ω, and imaginary part component varies from negative to positive. Hence, the resonance modes of the notch structure slot-1, slot-2, slot-3, left stub, and right stub can be actually represented by series RLC circuits. However, at 5.26 GHz the real part component is found to be 131 Ω, and imaginary part component varies from positive to negative which implies that a parallel resonant RLC circuit is required. The values of lumped RLC component values are evaluated with the aid of central notch frequency, quality factor, and bandwidth as given in Equations (4)–(6). The calculated values of resistor (R_i), Inductor (L_i) and capacitor (C_i) for each notch frequency are depicted in Table 2.

$$f_{notch,i} = \frac{1}{2\pi\sqrt{L_i C_i}} \tag{4}$$

$$Q_0 = \frac{1}{2\pi f_{notchi} R_i C_i} \tag{5}$$

$$BW = \frac{f_{notch,i}}{Q_0} \tag{6}$$

Table 2. Calculated RLC component values of the reported RLC equivalent circuit.

f (notch, i)	Bandwidth (GHz)	Quality factor (Q_0)	Resistor (Ω)	Inductor (nH)	Capacitor (pF)
First notch (3.41 GHz)	0.31	11	3.44	1.897	1.15
Second notch (3.84 GHz)	0.26	14.76	5.09	3.11	0.5519
Third notch (4.67 GHz)	0.17	27.4	24	22.456	0.0518
Fourth notch (5.26 GHz)	0.15	35	131	138.9	0.006602
Fifth notch (7.61 GHz)	0.27	28.18	19	0.112	0.03908
Sixth notch (9.44 GHz)	0.22	42.9	16	0.116	0.0245

2.4.2. Current Distribution

The band-notch principle of the suggested UWB-MIMO antenna could be studied most effectively by observing the surface current variation over the modified rectangular patch at the central notch frequencies of 3.41, 3.84, 4.67, 5.26, 7.61, and 9.44 GHz. By activating port-1 and terminating remaining ports, it is observed from Figs. 6(a)–(f) that the highest concentrations of current are found on the edges of slot-1 (at 3.41 GHz), slot-2 (at 3.84 GHz), slot-3 (at 4.67 GHz), slot-4 (at 5.26 GHz), right C-shape stub (at 7.61 GHz), and left C-shape stub (at 9.44 GHz) respectively and not elsewhere in the proposed array. Radiation fields are canceled out because currents will flow in opposite directions along the parallel edges of a specific band-notch arrangement. As a result, at the relevant band notch frequency, each band-notch structure operates as a non-radiator.

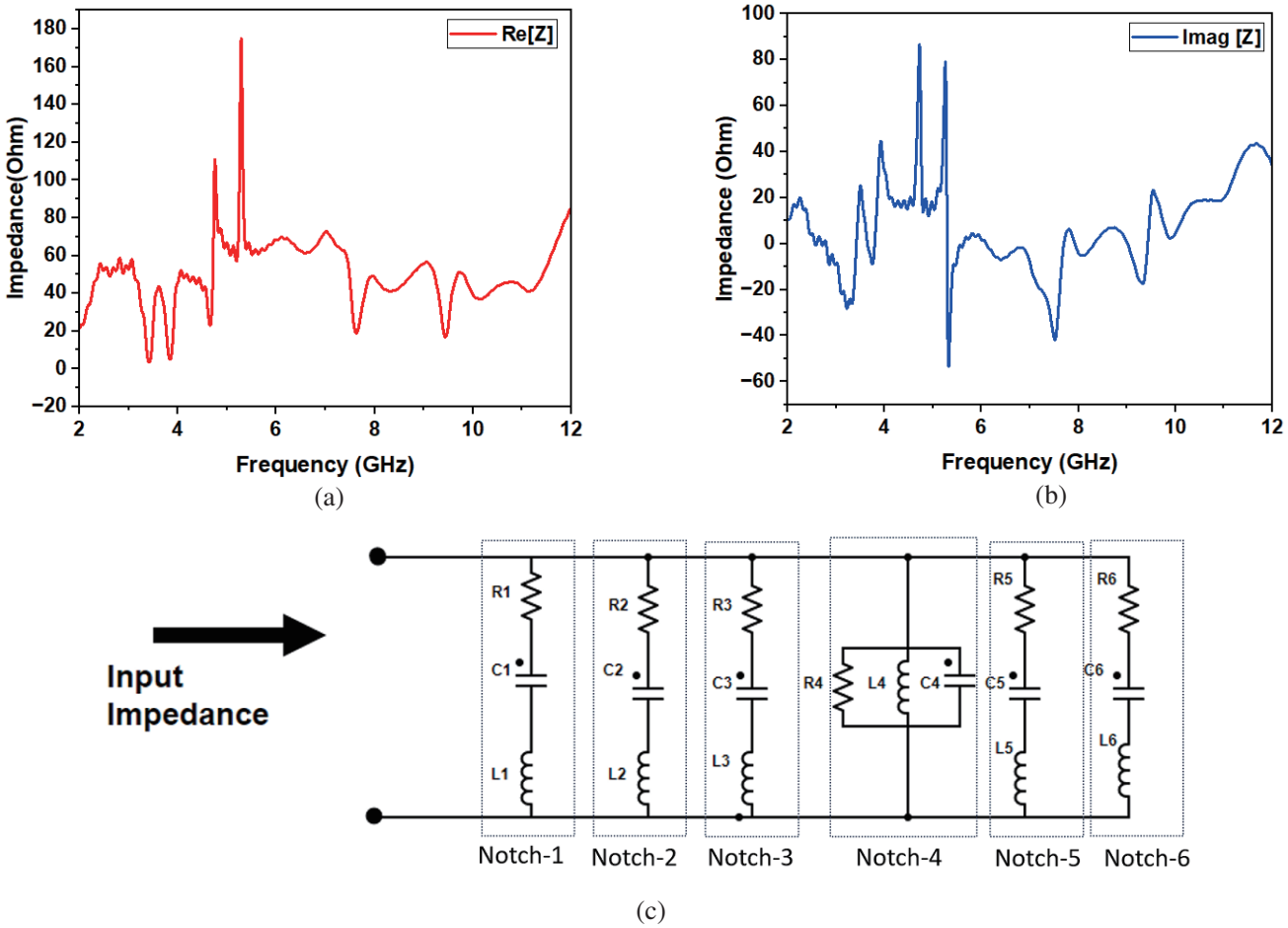

Figure 5. Impedance curves of the suggested band suppressed UWB-MIMO antenna. (a) Real component, (b) imaginary component, (c) lumped RLC equivalent circuit model.

3. RESULTS AND DISCUSSION

In this part, S-parameter experimental investigation for the fabricated model of the suggested UWB-MIMO antenna is reported (with Anirstu Vector Network Analyzer ranging from 5 kHz–15 GHz) along with far-field results (anechoic chamber ranges from 20 kHz to 20 GHz) to corroborate the practical implementation of the reported UWB-MIMO antenna for the mitigation of the intrusion caused by narrow-band systems.

3.1. Return Loss and Isolation Characteristics

Photographs of the investigation of the manufactured UWB-MIMO antenna for S_{11} and isolation S_{12} response are depicted in Figs. 7(a) and (b). Fig. 8 displays S_{11}, S_{12}, S_{13}, and S_{14} response curves from simulation and measurement. It is proved that the suggested array can successfully overcome the interference from six separate narrowband systems (WiMax, C-band, INSAT, WLAN, X-band, and Radio Navigation) that exists in the simulated as well as measured UWB range from 2.1–11.2 GHz (port-1) and 2.51–11.3 GHz (port-1), respectively.

3.2. Far-Field Results

The co-polar radiation properties of the reported UWB-MIMO antenna at passband frequencies of 3.61 GHz, 4.91 GHz, 5.64 GHz, and 7.92 GHz for port-1 excitation are illustrated in Fig. 9. The co-polar

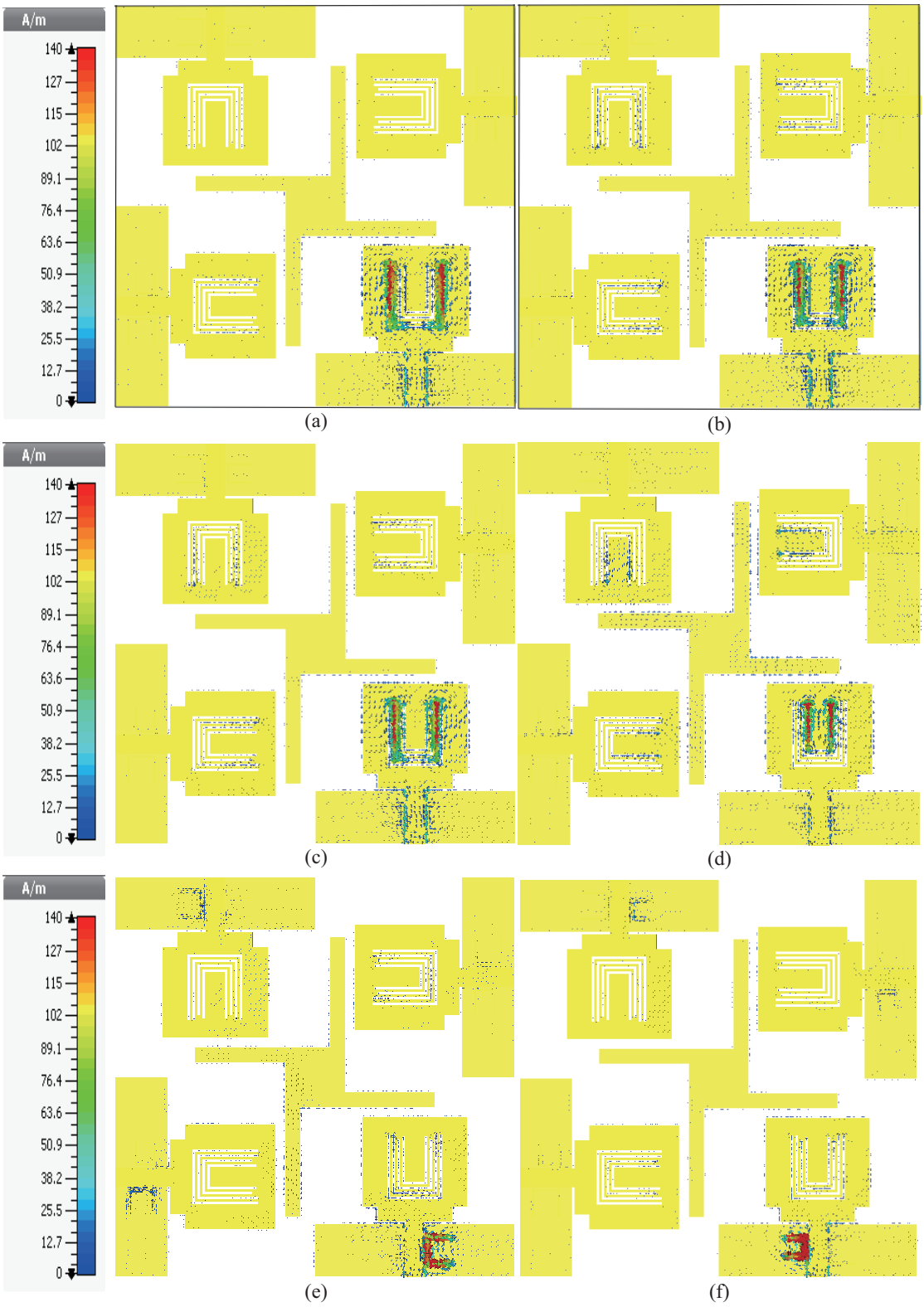

Figure 6. Surface current variation for the suggested quad port UWB-MIMO antenna (a) 3.41 GHz (b) 3.84 GHz (c) 4.67 GHz (d) 5.26 GHz (e) 7.61 GHz (f) 9.44 GHz.

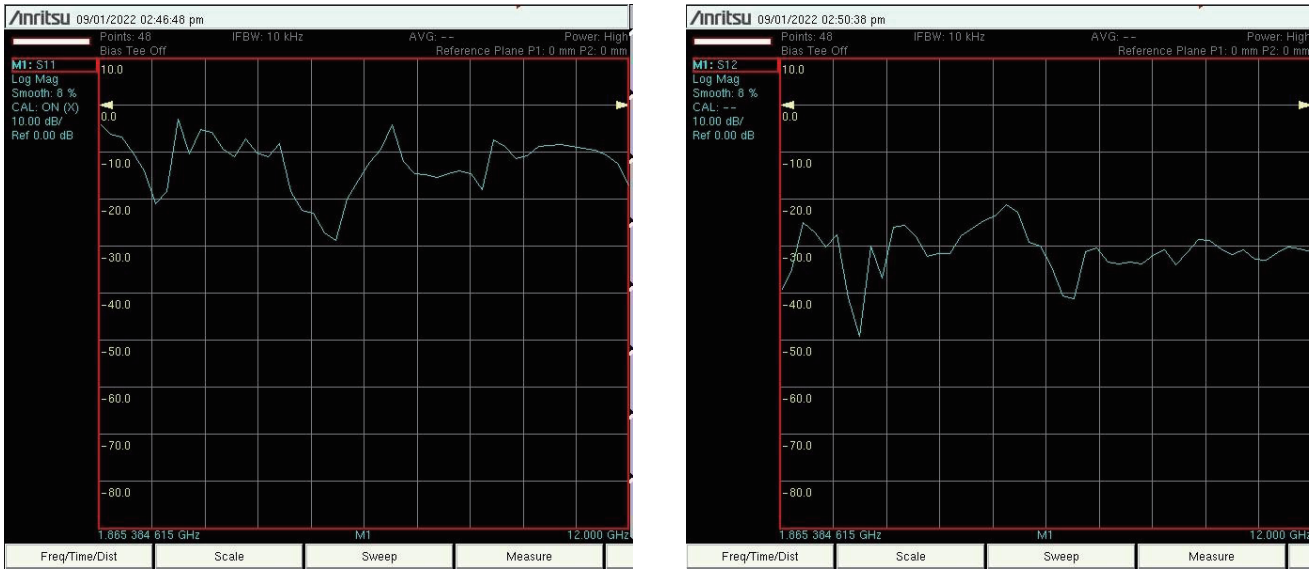

Figure 7. Photographs taken during the measurement of (a) S_{11} (dB) (b) S_{12} (dB).

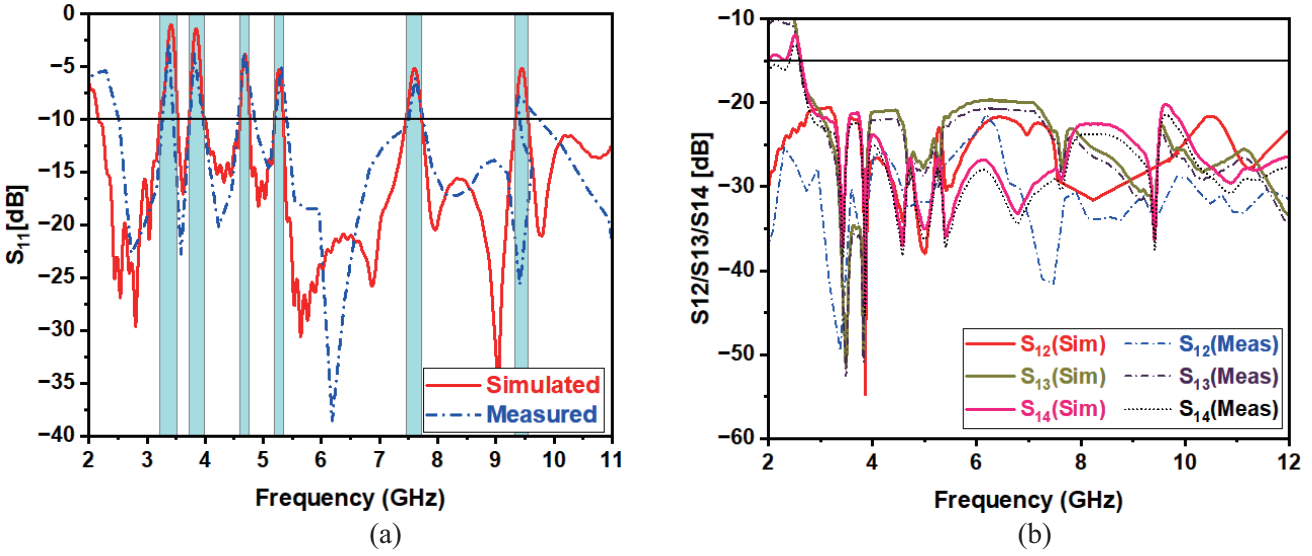

Figure 8. Simulated and experimental response of the reported UWB-MIMO antenna (a) S_{11} (dB) (b) S_{12} (dB).

simulated pattern curves provide evidence of the suggested antenna's reliable operation. The co-polar patterns in the E-plane were found to be bidirectional, whereas those in the H-plane were shown to be active in all directions. The concordance between simulated and experimental findings validates the design.

Figure 10(a) shows the gain comparison plot for the suggested UWB-MIMO antenna. It has been found that the simulated gain values correlate well with measured ones. The simulated and measured gains range from -0.75 to 6.7 dB with a less gain of -0.75 dB, -1 dB, -0.293 dB, -0.85 dB, -0.51 dB, and -1.5 dB at notch frequencies representing WiMAX, C-band, INSAT, WLAN, X-band, and radio navigation bands, respectively. The diminution of gain at central notch frequencies of 3.41, 3.84, 4.67, 5.26, 7.61, and 9.44 GHz is because of band rejection mechanism. Fig. 10(b) demonstrates simulated

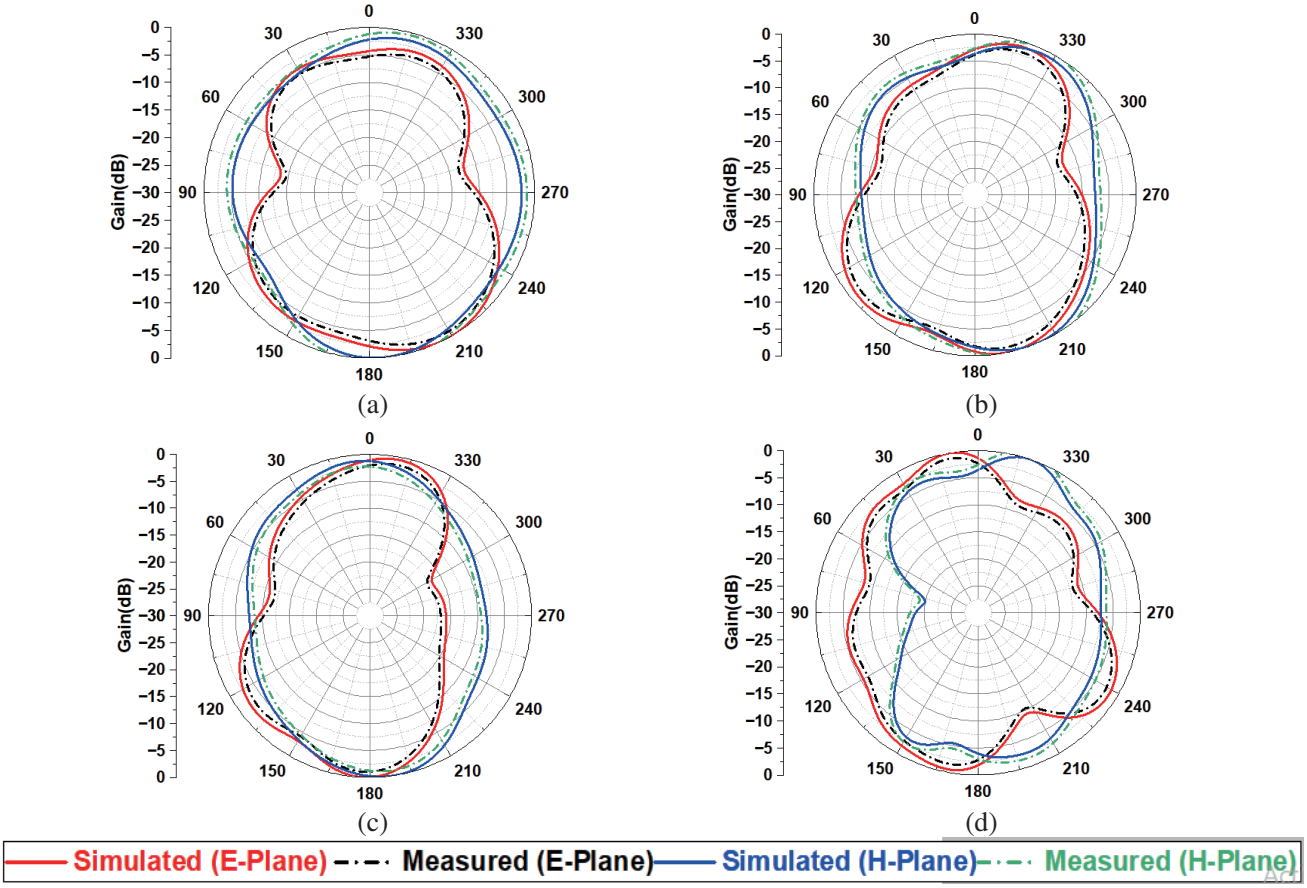

Figure 9. Normalized Radiation Patterns for the Pass band frequencies (a) 3.61 GHz (b) 4.91 GHz (c) 5.64 GHz (d) 7.92 GHz.

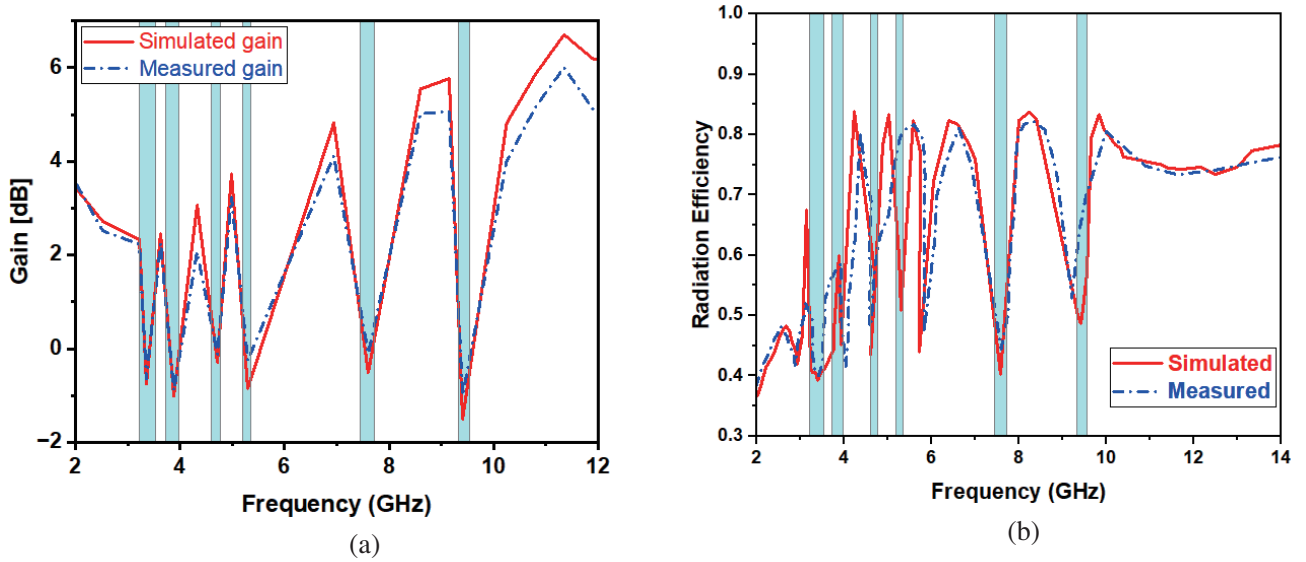

Figure 10. Variation of (a) broad band gain against frequency (b) radiation efficiency against frequency.

and measured radiation efficiencies for the reported antenna. It has stable efficiency of 83% throughout operating frequency. Contrarily, it drops to below 50% at notch frequencies.

4. ANALYSIS OF MIMO DIVERSITY CHARACTERISTICS

This section discusses numerous diversity performance measures such as envelope correlation coefficient (ECC), diversity gain (DG), mean effective gain (MEG), total active reflection coefficient (TARC), channel capacity loss (CCL) and multiplexing efficiency (ME) to evaluate the efficacy of the suggested UWB-MIMO antenna array in the scenario of multi path fading.

ECC is a vital diversity metric devised to quantify the coupling between neighbouring antenna elements by taking into consideration of the simulated 3-D radiation patterns on array performance. For array antennas to operate reliably in fading conditions, ECC should be less than 0.5. Mathematically, ECC can be computed by using 3-D radiation patterns of the MIMO array as shown in Equation (7).

$$\rho_{eij} = \frac{\left|\int_0^{2\pi}\int_0^{\pi}(XPR\cdot E\theta i\cdot E^*\theta j\cdot P\theta + E\varphi i\cdot E^*\varphi j\cdot P\varphi)d\Omega\right|^2}{\int_0^{2\pi}\int_0^{\pi}(XPR\cdot E\theta i\cdot E^*\theta i\cdot P\theta + E\varphi i\cdot E^*\varphi i\cdot P\varphi)d\Omega\times\int_0^{2\pi}\int_0^{\pi}(XPR\cdot E\theta j\cdot E^*\theta j\cdot P\theta + E\varphi j\cdot E^*\varphi j\cdot P\varphi)d\Omega} \tag{7}$$

Here i, j are port numbers; XPR is the cross-polarization ratio; P_θ and $P\varphi$ are θ and φ components of densityfunctions of incoming wave.

Figure 11(a) shows that simulated ECC is below 0.05 across the whole UWB range which signifies good diversity performance. DG is considered as an increase in signal to noise level (at the receiving end) brought on by the use of diversity schemes. Equation (8) shows the correlation between ECC and DG.

$$\mathrm{DG} = 10\sqrt{1-\mathrm{ECC}^2} \tag{8}$$

Figure 11(b) reveals that simulated DG is more than 9.8 dB for the entire operating band. Lower ECC and higher DG values imply that the suggested UWB-MIMO notched array has excellent diversity features for MIMO systems.

MEG is the primary parameter to be investigated in order to assess fading effects on MIMO antenna behavior in mobile applications. MEG is an average antenna gain in a real-world propagation scenario, and it can be calculated as

$$\mathrm{MEG}_i = 0.5\left[1-\sum_{j=1}^{N}|S_{ij}|^2\right] \leq -3\,\mathrm{dB} \tag{9}$$

$$\text{and} \qquad \mathrm{MEG}_1 - \mathrm{MEG}_2 \leq 3\,\mathrm{dB} \tag{10}$$

Figures 11(c) and (d) demonstrate that for the suggested MIMO configuration, the values of MEG1, MEG2, and MEG3 are less than 3 dB. The conditions of Equation (9) are met by the fact that the difference between MEG12 and MEG13 is less than 3 dB across the whole operating range. It connotes that the recommended UWB-MIMO antenna array offers the best diversity performance in a real-world applications.

Total active reflection coefficient (TARC) is a vital diversity parameter for characterizing MIMO performance as a function of impedance bandwidth and resonant frequency. It is the ratio of the square root of the whole reflected power to the incident power of the overall MIMO antenna system. Using Equation (10) TARC can be evaluated as

$$\mathrm{TARC} = \frac{\sqrt{\sum_{i=1}^{4}\left|S_{i1}+\sum_{n=2}^{4}S_{in}e^{j\theta n-1}\right|^2}}{2} \tag{11}$$

The TARC of the antenna is demonstrated in Fig. 11(e). It is noticed that TARC values are less than -10 dB over the usable frequency range when the notch frequencies are disregarded.

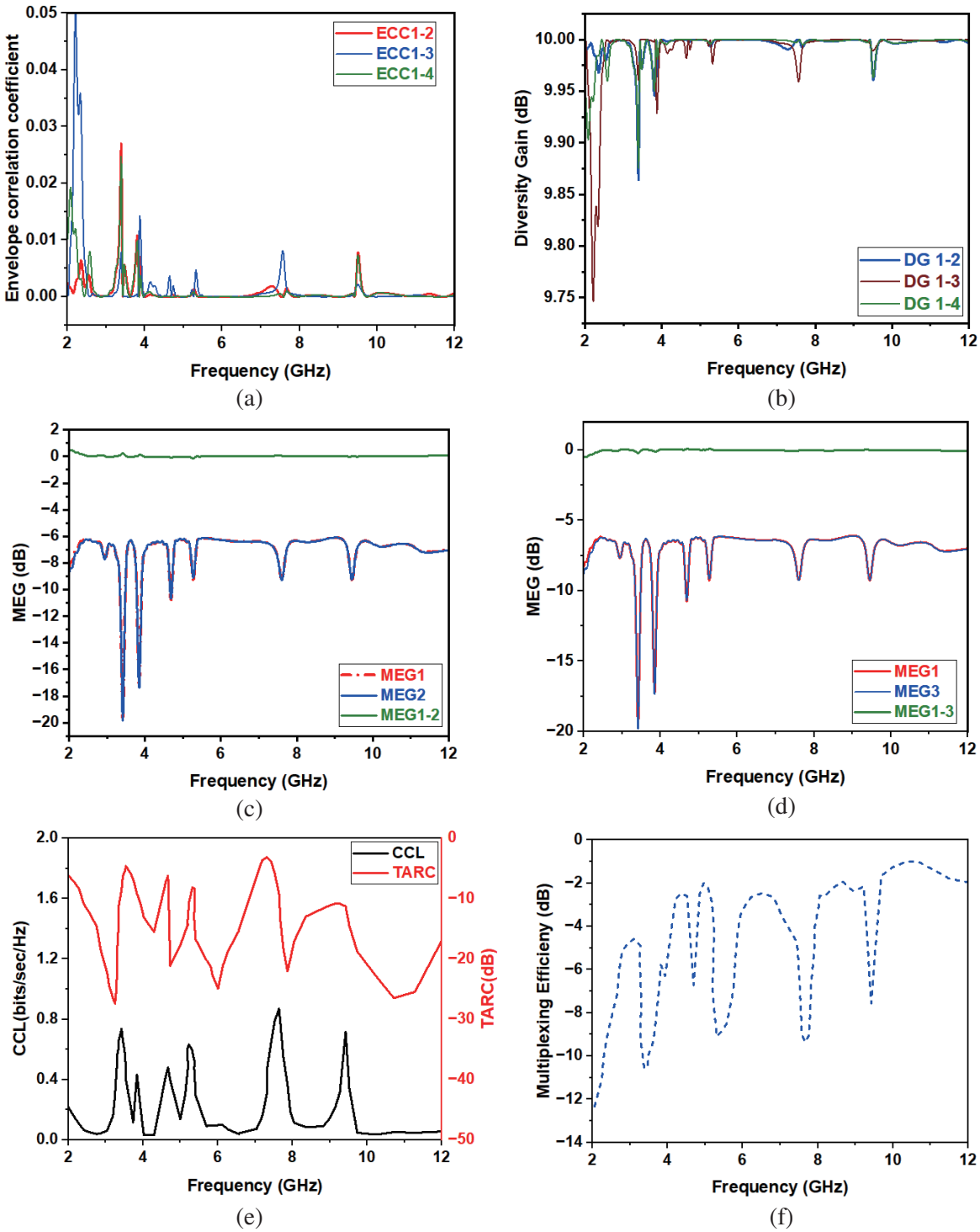

Figure 11. Variation in (a) ECC (b) DG (c) MEG between 1–2 (d) MEG between 1–3 (e) TARC and CCL (f) Multiplexing efficiency of the proposed UWB-MIMO antenna array.

In a multiple-input, multiple-output (MIMO) system, the channel capacity scales in proportion with number of antenna elements deployed. There are, nevertheless, some losses involved because of the correlated MIMO channels. In MIMO systems, channel capacity loss is caused by correlation between elements. Thus, CCL is a crucial metric for defining the MIMO system's channel capacity. The CCL of

the antenna is demonstrated in Fig. 11(e). For a MIMO system, the intended value of the CCL is below 0.4 bps/Hz. It is noticed that apart from six notch frequencies, the CCL is less than 0.2 bps/Hz for the entire impedance bandwidth. The multiplexing efficiency of the (η_{mux}) is calculated by the following Equation (11).

$$\eta_{mux} = \sqrt{\eta_i \eta_j (1 - |\rho_c|^2)} \tag{12}$$

From Fig. 11(f), it is concluded that multiplexing efficiency has hexa-band notch characteristics. For the whole impedance bandwidth (2.1–11.2 GHz) except for notch frequencies, the multiplexing efficiency is greater than −3 dB (4.2–12 GHz), and it is less than −3 dB at lower frequencies (2–4.2 GHz) only, which signifies that UWB-MIMO antenna has high multiplexing efficiency. Table 3 compares several aspects of the proposed study with state of art models to illustrate the significance of the suggested research.

Table 3. Performance comparison of the suggested UWB-MIMO antenna with state of art antenna designs.

Ref.	BW (GHz)	No. of Notches	Peak Gain (dBi)	Isolation (dB)	ECC	CCL (bps/Hz)	TARC	Multiplexing Efficiency	No. Of Ports	Size
[9]/2022	4–12	NA	5.57	> 19	< 0.2	< 0.2	0	> -3 dB	2	$0.34\lambda_0 \times 0.22\lambda_0$
[13]/2017	2.5–14.5	NA	4	> 20	< 0.04	NA	NA	NA	2	$0.41\lambda_0 \times 00.25\lambda_0$
[18]/2015	2–10.6	1	4	> 17	< 0.005	< 0.3	NA	NA	4	$0.3\lambda_0 \times 00.3\lambda_0$
[20]/2017	3.08–10.98	1	5	> 20	< 0.013	< 0.35	< -10	NA	2	$0.3\lambda_0 \times 00.3\lambda_0$
[21]/2022	3.4–12.1	2	4.4	> 16	< 0.001	NA	< -10	> -2 dB	2	$0.24\lambda_0 \times 00.31\lambda_0$
[22]/2020	3.1–10.6	2	2.91	> 18	< 0.13	< 0.4	< -10	NA	2	$0.19\lambda_0 \times 00.31\lambda_0$
[25]/2018	2.5–11	3	6	> 15	< 0.02	NA	NA	NA	2	$0.53\lambda_0 \times 00.37\lambda_0$
[26]/2022	3.07–12.40	3	4.6	> 22	< 0.001	NA	NA	NA	2	$0.18\lambda_0 \times 00.34\lambda_0$
[29]/2021	3–10.7	4	5.3	> 25	< 0.01	NA	NA	NA	2	$0.43\lambda_0 \times 00.35\lambda_0$
[30]/2016	2.7–12	1	5.7	> 17	< 0.03	NA	NA	NA	4	$0.45\lambda_0 \times 00.36\lambda_0$
Proposed	**2.1–11.2**	**6**	**6.6**	$\mathbf{> 20}$	$\mathbf{< 0.02}$	$\mathbf{< 0.2}$	$\mathbf{< -13}$	$\mathbf{> -3}$ **dB**	**4**	$\mathbf{0.55\lambda_0 \times 0.55\lambda_0}$

5. CONCLUSION

This paper models and investigates a four port UWB-MIMO antenna with sextuple band suppression characteristics. The suggested UWB-MIMO antenna employs four modified rectangle-shaped patch elements along with a groove over partial ground and is designed to attain an enhanced isolation among antenna ports. Furthermore, four U-shaped slots are etched from the radiators and a pair of C-shaped stubs adjacent to feed-line to mitigate the interference caused by WiMAX, C-band, INSAT, WLAN, X-band, and Radio navigation bands, respectively. Band rejection principle of the suggested UWB-MIMO antenna is assisted by its RLC equivalent circuit and surface current variation at the intended notch frequencies. Broad band gain varies in the range −0.75–6.6 dB with minute values of gain observed at notch frequencies. For receiving diversity techniques, the reported UWB-MIMO antenna system provides an ECC < 0.05, high DG (≥ 9.99), MEG ≤ -3.01 dB, TARC < -10 dB, and ME > -3 dB over the whole operating frequency except at notches. The computed and experimental MIMO antenna performances (particularly operating bandwidth, isolation, far-field characteristics, and diversity performance parameters) are well matched, which supports the proposed MIMO antenna's functioning in a real scenario. As a result, the suggested array's suitability to miniature UWB-MIMO systems is validated by its compactness, large fractional bandwidth, high isolation, mitigation of intrusion frequency bands, steady radiation properties, and strong diversity behavior.

REFERENCES

1. Federal Communications Commission: Revision of Part 15 of the Commission's Rules Regarding Ultra-Wideband Transmission System from 3.1 to 10.6 GHz, Federal Communications Commission, Washington, DC, ET-Docket, 98–153, 2002.
2. Liu, L., S. W. Cheung, and T. I. Yuk, "Compact MIMO antenna for portable devices in UWB applications," *IEEE Transactions on Antennas and Propagation*, Vol. 61, No. 8, 4257–4264, 2013.
3. Assa, M. and S. Ramesh, "UWB MIMO antenna for interference reduction in wireless communications," *Telecommunications and Radio Engineering*, Vol. 76, No. 15, 2017.
4. Zhang, S. and G. F. Pedersen, "Mutual coupling reduction for UWB MIMO antennas with a wideband neutralization line," *IEEE Antennas and Wireless Propagation Letters*, Vol. 15, 166–169, 2016.
5. Su, S.-W., C.-T. Lee, and F.-S. Chang, "Printed MIMO-antenna system using neutralization-line technique for wireless USB-dongle applications," *IEEE Transactions on Antennas and Propagation*, Vol. 60, No. 2, 456–463, 2012.
6. Vasu Babu, K. and B. Anuradha, "Design of Wang shape neutralization line antenna to reduce the mutual coupling in MIMO antennas," *Analog. Integr. Circ. Sig. Process.*, Vol. 101, 67–76, 2019.
7. Sun, Y., M. Tian, and G. S. Cheng, "Characteristics mode based neutralization line design for MIMO antenna," *International Journal of Antennas and Propagation*, Vol. 2022, 1–14, 2022.
8. Quevedo-Teruel, O., L. Inclan-Sanchez, and E. Rajo-Iglesias, "Soft surfaces for reducing mutual coupling between loaded PIFA antennas," *IEEE Antennas and Wireless Propagation Letters*, Vol. 9, 91–94, 2010.
9. Urimubenshi, F., D. B. O. Konditi, J. de Dieu Iyakaremye, P. M. Mpele, and A. Munyaneza, "A novel approach for low mutual coupling and ultra-compact two port MIMO antenna development for UWB wireless application," *Heliyon*, Vol. 8, No. 3, 2022.
10. Wang, H., D. G. Fang, and X. L. Wang, "Mutual coupling reduction between two microstrip patch antennas by using the parasitic elements," *Asia-Pacific Microwave Conference*, 1–4, 2008.
11. Acharjee, J., K. mandal, and S. K. Mandal, "Reduction of mutual coupling and cross-polarization of a MIMO/diversity antenna using a string of H-shaped DGS," *International Journal of Electronics and Communications*, Vol. 97, 110–119, 2018.
12. Radhi, A., R. Nilavalan, Y. Wang, H. Al-Raweshidy, A. Eltokhy, and N. Ab Aziz, "Mutual coupling reduction with a wideband planar decoupling structure for UWB-MIMO antennas," *International Journal of Microwave and Wireless Technologies*, Vol. 10, No. 10, 1143–1154, 2018.
13. Ali, W. A. E. and A. A. Ibrahim, "A compact double-sided MIMO antenna with an improved isolation for UWB applications," *AEU-Int. J. Electron. Commun.*, Vol. 82, 7–13, Dec. 2017.
14. Lee, Y., D. Ga, and J. Choi, "Design of a MIMO antenna with improved isolation using MNG metamaterial," *International Journal of Antennas and Propagation*, Vol. 2012, 1–7, 2012.
15. Khan, M. K., Q. Feng, and Z. Zheng, "Experimental investigation and design of UWB MIMO antenna with enhanced isolation," *Progress In Electromagnetics Research C*, Vol. 107, 287–297, 2021.
16. Iqbal, A., O. A. Saraereh, A. W. Ahmad, and S. Bashir, "Mutual coupling reduction using F-shaped stubs in UWB-MIMO antenna," *IEEE Access*, Vol. 6, 2755–2799, 2018.
17. Zhu, J., S. Li, B. Feng, L. Deng, and S. Yin, "Compact dual-polarized UWB quasi-self-complementary MIMO/diversity antenna with band-rejection capability," *IEEE Antennas and Wireless Propagation Letters*, Vol. 15, 905–908, 2016.
18. Tripathi, S., A. Mohan, and S. Yadav, "A compact koch fractal UWB MIMO antenna with WLAN band-rejection," *IEEE Antennas and Wireless Propagation Letters*, Vol. 14, 1565–1568, 2015.
19. Khan, M. S., B. D. Braaten, A. Iftikhar, A. D. Capobianco, B. Ijaz, and S. Asif, "Compact 4×4 UWB-MIMO antenna with WLAN band rejected operation," *Electronics Letters*, Vol. 51, 1048–1050, 2015.

20. Biswal, S. P. and S. Das, "A low-profile dual port UWB-MIMO/diversity antenna with band rejection ability," *International Journal of RF and Microwave Computer Aided Engineering*, Vol. 28, No. 1, 2017.
21. Kumar, P., T. Ali, and M. M. Manohara, "Characteristic mode analysis-based compact dual band-notched UWB MIMO antenna loaded with neutralization line," *Micromachines*, Vol. 13, 1599, 2022.
22. Kumar, A., Q. A. Ansari, K. B. Kanaujia, J. Kishor, and S. Kumar, "An ultra compact two-port UWB MIMO antenna with dual band notched characteristics," *AEU-International Journal of Electronics and Communications*, Vol. 114, 1–12, 2020.
23. Kadam, A. A. and A. A. Deshmukh, "Pentagonal shaped UWB antenna loaded with slot and EBG structure for dual band notched response," *Progress In Electromagnetics Research M*, Vol. 95, 165–176, 2020.
24. Mandal, T. and S. Das, "Design and analysis of triple notch band UWB monopole antenna using mushroom structure," *Telecommunications and Radio Engineering*, Vol. 79, No. 6, 2020.
25. Jaglan, N., S. D. Gupta, E. Thakur, D. Kumar, B. K. Kanaujia, and S. Srivastava, "Triple band notched mushroom and uniplanar EBG structures based UWB MIMO/diversity antenna with enhanced wide band isolation," *AEU-International Journal of Electronics and Communications*, Vol. 90, 36–44, 2018.
26. Khan, M. K. and Q. Feng, "Design validation of UWB MIMO antenna with enhanced isolation and novel strips for stop-band characteristics," *Entropy*, Vol. 24, 6766, 2022.
27. Chen, Z., W. Zhou, and Z. Hong, "A miniaturized MIMO antenna with triple band-notched characteristics for UWB applications," *IEEE Access*, Vol. 9, 63646–63655, 2021.
28. Kumar, P., S. Urooj, and F. Alrowais, "Design of quad-port MIMO/diversity antenna with triple-band elimination characteristics for super-wide band applications," *Sensors*, Vol. 20, 1–12, 2020.
29. Modak, S. and T. Khan, "A slotted UWB-MIMO antenna with quadruple band-notch characteristics using mushroom EBG structure," *International Journal of Electronics and Communications*, Vol. 134, 1–6, 2021.
30. Khan, S. M., A. Iftikhar, S. M. Asif, A.-D. Capobianco, and B. D. Braaten, "A compact four elements UWB MIMO antenna with on-demand WLAN rejection," *Microw. Opt. Technol. Lett.*, Vol. 58, No. 2, 270–276, Feb. 2016.